PHYSICAL REVIEW D VOLUME 52, NUMBER 10 15 NOVEMBER 1995

Evolution of three-dimensional gravitational waves: Harmonic slicing case

Masaru Shibata
Department of Earth and Space Science, Faculty of Science, Osaka University, Toyonaka, Osaka 560, Japan

Takashi Nakamura
Yukawa Institute for Theoretical Physics, Kyoto University, Kyoto 606-01, Japan
(Received 7 April 1995)

We perform numerical simulations of a three-dimensional (3D) time evolution of pure gravitational waves. We use a conformally flat and $K = 0$ initial condition for the evolution of the spacetime. We adopt several slicing conditions to check whether a long time integration is possible in those conditions. For the case in which the amplitude of the gravitational waves is low, a long time integration is possible by using the harmonic slice and the maximal slice, while in the geodesic slice ($\alpha = 1$) it is not possible. As in the axisymmetric case and also in the 3D case, gravitational waves with a sufficiently high amplitude collapse by their self-gravity and their final fates seem to be as black holes. In this case, the singularity avoidance property of the harmonic slice seems weak, so that it may be inappropriate for the formation problems of the black hole. By means of the gauge-invariant wave extraction technique we compute the waveform of the gravitational waves at an outer region. We find that the nonlinearity of Einstein gravity induces the higher multipole modes even if only a quadrupole mode exists initially.

PACS number(s): 04.30.Nk

I. INTRODUCTION

Gravitational waves from the last three minutes of coalescing compact binary systems [1] (neutron-star–neutron-star, black-hole–neutron-star, and black-hole–black-hole binaries) are one of the main targets of the kilometer-size laser interferometric gravitational wave detectors such as the Laser Interferometric Gravitational Wave Observatory (LIGO) [2] and VIRGO [3]. These binaries first emit quasiperiodic gravitational waves. During this stage, the emission time scale of gravitational waves is much longer than that of the orbital period, so that we may assume the adiabatic evolution of the binary. However, once two stars in the binary approach up to $\sim$ 6–8 M, where M is the total mass of the binary, they cannot maintain the circular orbit because the centrifugal force cannot be balanced with the strong relativistic gravity [4] or tidal force [5]. At this stage, the circular orbit of the binary changes to the plunge one, and finally they emerge and will become a rotating black hole in a few milliseconds. In such a phase, i.e., in the *last three milliseconds of a coalescing binary*, many gravitational waves will be emitted violently [6], and these gravitational waves reflect the strong gravitational field and the fast motion of the matter there. Hence, if we can detect such gravitational waves by LIGO and VIRGO, we will be able to see a strong gravitational field.

Such gravitational waves, however, have a frequency of $\sim$ kHz, so that the sensitivity of the laser interferometric detectors will not be so high (the signal-to-noise ratio is at most 10) even for advanced LIGO [2]. To confirm the detection of such a signal of gravitational waves, we had better prepare a theoretical template of gravitational waves which can be compared with the detected signal of gravitational waves. Here, any approximations in general relativity break down to calculate gravitational waves at the binary merging. We must solve the fully general relativistic equations, which can be done only by a three-dimensional (3D) numerical simulation. This paper is an effort toward the success of such simulations.

In 3D numerical relativity, there are several points to be developed. One of them is the choice of an appropriate spatial gauge and slicing condition, and another is the establishment of the method to extract gravitational waves from the 3D metric. As for the spatial gauge, we require that it should be free from an appearance of coordinate singularity as well as that it deletes the spurious gauge modes. The minimal distortion (MD) gauge was proposed by Smarr and York [7] seventeen years ago as a spatial gauge which has the required property. However, to adopt it, we must solve the complicated vector Laplacian equation and no one has tried to use it except in spherically symmetric calculations. Recently, one of us (T.N.) used a similar type gauge condition (which we call a pseudominimal shear gauge) for test simulations of merging binary neutron stars, rotating core collapse, and the head on collision of two black holes, and made sure that this type of gauge condition is a good one [8].

As for a slicing condition, we require that it should have the following two properties: the first is a singularity avoidance property, and the second is that a long time integration is possible by using it. The maximal slice ($K = 0$, where K is the trace part of the extrinsic curvature) is a well-known slicing condition which has the singularity avoidance property. However, to adopt this slicing condition, we need to solve a 3D elliptical equation that is somewhat time consuming. Shibata and Nakamura proposed the conformal slice which seems to be appropriate in order to see gravitational waves in the

wave zone. This slicing condition also has the singularity avoidance property for the formation problem of the black hole [9]. T. N. used the conformal slice for simulations of merging binary neutron stars and rotating core collapse, and found that the conformal slice has an excellent property to see gravitational waves in the wave zone [8]. However, as shown in Sec. IV B, this slicing condition is not good for pure gravitational wave problems.

Recently, the harmonic slice ($\Box t = 0$) has been proposed [10]. The harmonic slice seems to have the singularity avoidance property [10] and is very tractable because we only need to solve a simple evolution equation for the lapse function. However, this slicing condition has not been investigated much compared with other slicing conditions and the detailed properties have not been known well. We hope to clarify in what problems we can use it.

As for the wave extraction, recently, the gauge-invariant wave extraction technique has been developed by NCSA group [11]. In their method, they assume that the numerically calculated spacetime metric in the wave zone can be split into the Schwarzschild metric and the metric of the linear part. Then, they calculate the gauge-invariant quantity from the linear part. Using this technique, they calculated the quasinormal modes clearly in their axisymmetric calculations of black hole spacetimes. We need to check this technique for 3D calculations whether we can extract the wave form clearly.

For these purposes, we simulate the evolution of the 3D vacuum spacetime of pure gravitational waves in this paper. To check the behavior of the spacetime under several slicing conditions and to investigate that the wave extraction technique works well for various situations, we consider low amplitude gravitational waves as well as a high amplitude one. The paper is organized as follows. We describe the basic equations as well as the boundary conditions and the numerical methods in Sec. II. In Sec. III, we show conformally flat and $K = 0$ initial conditions of gravitational waves. In Sec. IV, we investigate the property of several slicing conditions. In this paper we adopt the geodesic slice ($\alpha = 1$, where α is the lapse function), harmonic slice, and the maximal slice. We will show the advantages and disadvantages of them, briefly. In Sec. V, we first describe the methods for the analysis of numerical data and then show numerical results. It is found that the singularity avoidance property of the harmonic slice is weak. Section VI is devoted to summary.

Throughout this paper, we use the units of $c = 1$, and Greek and Latin indices take 0, 1, 2, 3 and $i = 1, 2, 3$, respectively.

II. FORMULATION

In this paper, the basic equation is the vacuum Einstein equation as

$$G_{\mu\nu} = 0 \ . \tag{2.1}$$

We solve this equation imposing no symmetries except for the equatorial plane symmetry. To solve Eq. (2.1), we use the (3+1) formalism and write the line element as

$$ds^2 = -(\alpha^2 - \beta_i\beta^i)dt^2 + 2\beta_i dt\, dx^i + \gamma_{ij}dx^i dx^j \ , \tag{2.2}$$

where α, β^j and γ_{ij} are the lapse function, the shift vector and the metric on a 3D hypersurface, respectively. Using the 3+1 formalism, the Einstein equation is split into the constraint equations and the evolution equations. The Hamiltonian and momentum constraints are

$$R - K_{ij}K^{ij} + K^2 = 0 \ , \tag{2.3}$$

$$D_i K^i{}_j - D_j K = 0 \ , \tag{2.4}$$

where K_{ij}, K, R, and D_i are the extrinsic curvature, the trace part of K_{ij}, the scalar curvature of a 3D hypersurface and the covariant derivative with respect of γ_{ij}, respectively. Evolution equations for the metric and extrinsic curvature are, respectively, written as

$$\frac{\partial}{\partial t}\gamma_{ij} = -2\alpha K_{ij} + D_i\beta_j + D_j\beta_i \ , \tag{2.5}$$

$$\frac{\partial}{\partial t}K_{ij} = \alpha(R_{ij} + KK_{ij} - 2K_{ij}K^l_j) - D_iD_j\alpha + (D_j\beta^m)K_{mi} + (D_i\beta^m)K_{mj} + \beta^m D_m K_{ij} \ , \tag{2.6}$$

$$\frac{\partial}{\partial t}\ln(\gamma) = -2\alpha K + 2D_i\beta^i \ , \tag{2.7}$$

$$\frac{\partial}{\partial t}K = \alpha(R + K^2) - D^iD_i\alpha + \beta^j D_j K \ , \tag{2.8}$$

where R_{ij} and γ are the Ricci tensor with respect to γ_{ij} and determinant of γ_{ij}, respectively. Hereafter we use $\phi = \ln(\gamma)/12$ instead of γ.

Although it is possible to treat these evolution equations for numerical integration, in our numerical code we solve $\tilde{\gamma}_{ij} = \exp(-4\phi)\gamma_{ij}$ instead of γ_{ij} for convenience and define $\det(\tilde{\gamma}_{ij})$ to be unity. We also define $\tilde{A}_{ij}$ as

$$\tilde{A}_{ij} \equiv \exp(-4\phi)A_{ij} \equiv \exp(-4\phi)(K_{ij} - \tfrac{1}{3}\gamma_{ij}K) \ . \tag{2.9}$$

We should note that in our notation, indices of $\tilde{A}_{ij}$ are raised and lowered by $\tilde{\gamma}_{ij}$, so that the relations, $\tilde{A}^i{}_j = A^i{}_j$ and $\tilde{A}^{ij} = \exp(4\phi)A^{ij}$, hold. Using these variables, the evolution equations (2.5)–(2.8) can be rewritten as

$$\frac{d}{dt}\tilde{\gamma}_{ij} = -2\alpha\tilde{A}_{ij} + \tilde{\gamma}_{il}\frac{\partial\beta^l}{\partial x^j} + \tilde{\gamma}_{jl}\frac{\partial\beta^l}{\partial x^i} - \frac{2}{3}\tilde{\gamma}_{ij}\frac{\partial\beta^l}{\partial x^l} \ , \tag{2.10}$$

$$\frac{d}{dt}\tilde{A}_{ij} = \exp(-4\phi)\left[\alpha\left(R_{ij} - \frac{1}{3}\gamma_{ij}R\right) - \left(D_iD_j\alpha - \frac{1}{3}\gamma_{ij}D^kD_k\alpha\right)\right] + \alpha(K\tilde{A}_{ij} - 2\tilde{A}_{il}\tilde{A}^l{}_j) + \frac{\partial\beta^m}{\partial x^i}\tilde{A}_{mj} + \frac{\partial\beta^m}{\partial x^j}\tilde{A}_{mi} + \frac{2}{3}\frac{\partial\beta^m}{\partial x^m}\tilde{A}_{ij} \ , \tag{2.11}$$

$$\frac{d}{dt}\phi = \frac{1}{6}\left(-\alpha K + \frac{\partial \beta^i}{\partial x^i}\right) , \tag{2.12}$$

$$\frac{d}{dt}K = \alpha(\tilde{A}_{ij}\tilde{A}^{ij} + \tfrac{1}{3}K^2) - D^i D_i \alpha , \tag{2.13}$$

where

$$\frac{d}{dt} = \frac{\partial}{\partial t} - \beta^i \frac{\partial}{\partial x^i} . \tag{2.14}$$

Now let us consider R_{ij} which is the main source term of the evolution equation for $\tilde{A}_{ij}$. First we split R_{ij} into two parts as

$$R_{ij} = \tilde{R}_{ij} + R^{\phi}_{ij} , \tag{2.15}$$

where $\tilde{R}_{ij}$ is the Ricci tensor with respect to $\tilde{\gamma}_{ij}$ and R^{ϕ}_{ij} is given as

$$\begin{aligned} R^{\phi}_{ij} = & -2\tilde{D}_i\tilde{D}_j\phi - 2\tilde{\gamma}_{ij}\tilde{D}^k\tilde{D}_k\phi + 4(\tilde{D}_i\phi)(\tilde{D}_j\phi) \\ & -4\tilde{\gamma}_{ij}(\tilde{D}_k\phi)(\tilde{D}^k\phi) , \end{aligned} \tag{2.16}$$

with $\tilde{D}_i$ being the covariant derivative with respect to $\tilde{\gamma}_{ij}$. Using the property of $\det(\tilde{\gamma}_{ij}) = 1$, $\tilde{R}_{ij}$ is written as

$$\begin{aligned} \tilde{R}_{ij} = & \tfrac{1}{2}[\tilde{\gamma}^{kl}(\tilde{\gamma}_{lj,ik} + \tilde{\gamma}_{li,jk} - \tilde{\gamma}_{ij,lk}) + \tilde{\gamma}^{kl}{}_{,k}(\tilde{\gamma}_{lj,i} \\ & +\tilde{\gamma}_{li,j} - \tilde{\gamma}_{ij,l})] - \tilde{\Gamma}^l_{kj}\tilde{\Gamma}^k_{li} , \end{aligned} \tag{2.17}$$

where $,i$ denotes $\partial/\partial x^i$ and $\tilde{\Gamma}^k_{ij}$ is the Christoffel symbol with respect to $\tilde{\gamma}_{ij}$. Following Nakamura and co-workers [12], we split $\tilde{\gamma}_{ij}$ and $\tilde{\gamma}^{ij}$ as $\eta_{ij} + h_{ij}$ and $\eta^{ij} + f^{ij}$, where η_{ij} denotes the flat geometry, and rewrite $\tilde{R}_{ij}$ as

$$\begin{aligned} \tilde{R}_{ij} = & \tfrac{1}{2}[-h_{ij,kk} + h_{jl,li} + h_{il,lj} \\ & +f^{kl}{}_{,k}(h_{lj,i} + h_{li,j} - h_{ij,l}) \\ & +f^{kl}(h_{lj,ik} + h_{li,jk} - h_{ij,lk})] - \tilde{\Gamma}^l_{kj}\tilde{\Gamma}^k_{li} . \end{aligned} \tag{2.18}$$

As shown by Nakamura and co-workers [12], the first term is the main part of the wave equation, that is, in the linear approximation of the vacuum Einstein equation, it appears irrespective of the gauge condition. The other terms are nonlinear terms or gauge terms in the linear approximation; i.e., the second and third terms are the gauge terms or have essentially the nonlinear nature. This is because the source terms of the evolution equation for $h_{ij,j}$ are either the nonlinear terms or the gauge terms [see Eq. (2.20)], and if we take the linear approximation, we can set them zero. To guarantee the nonlinearity of them as well as to avoid the appearance of the spurious wave terms, we introduce a new variable as

$$F_i \equiv h_{ij,j} , \tag{2.19}$$

and rewrite the second and third terms of $\tilde{R}_{ij}$ as $F_{i,j} + F_{j,i}$. Using the momentum constraint equation, the evolution equation of F_i can be written as

$$\begin{aligned} \frac{d}{dt}F_i = & 2\alpha(f^{kj}\tilde{A}_{ik,j} + f^{kj}{}_{,j}\tilde{A}_{ik} - \tfrac{1}{2}\tilde{A}^{jl}h_{lj,i} \\ & +6\phi_{,k}\tilde{A}^k{}_i - \tfrac{2}{3}K_{,i}) - 2\alpha_{,j}\tilde{A}_{ij} + \beta^k{}_{,j}h_{ij,k} \\ & +(\tilde{\gamma}_{il}\beta^l{}_{,j} + \tilde{\gamma}_{jl}\beta^l{}_{,i} - \tfrac{2}{3}\tilde{\gamma}_{ij}\beta^l{}_{,l})_{,j} . \end{aligned} \tag{2.20}$$

Now, Eqs. (2.10)–(2.13) and (2.20) are the evolution equations to be solved.

To solve them, we must specify a slice and spatial gauge condition for α and β^i, respectively. In our numerical code, any choices of the slice and spatial gauge conditions are possible. However in the present paper, we choose $\beta^i = 0$ as the spatial gauge condition for simplicity. In general cases such as the simulation of coalescing binary neutron stars, we should consider an appropriate spatial gauge condition such as minimal distortion gauge [8]. On the other hand, we adopt several slicing conditions to test them; geodesic slice, harmonic slice, algebraic slice similar to the harmonic slice [$\alpha \propto \exp(n\phi)$; n is an integer] and maximal slice. We discuss their properties in the subsequent section (see Sec. IV).

In the numerical simulation, we use the Cartesian grid, so the components of the metric and extrinsic curvature which appear in the numerical code are $\tilde{\gamma}_{xx}$, $\tilde{\gamma}_{xy}$, ... and $\tilde{A}_{xx}$, $\tilde{A}_{xy}$, ... Since we assume the equatorial plane symmetry, the following relations of symmetry hold:

$$\begin{aligned} & \phi(z) = \phi(-z), \quad \alpha(z) = \alpha(-z) , \\ & \tilde{\gamma}_{ab}(z) = \tilde{\gamma}_{ab}(-z), \quad \tilde{\gamma}_{zz}(z) = \tilde{\gamma}_{zz}(-z) , \\ & \tilde{A}_{ab}(z) = \tilde{A}_{ab}(-z), \quad \tilde{A}_{zz}(z) = \tilde{A}_{zz}(-z) , \\ & \tilde{\gamma}_{az}(z) = -\tilde{\gamma}_{az}(-z), \quad \tilde{A}_{az}(z) = -\tilde{A}_{az}(-z) , \\ & F_a(z) = F_a(-z), \quad F_z(z) = -F_z(-z) , \end{aligned} \tag{2.21}$$

where a and b denote x or y.

As for the outer boundary condition, we use the following one for $\tilde{\gamma}_{ij}$, F_i, ϕ, and $\tilde{A}_{ij}$:

$$rQ(u) = \text{const} , \tag{2.22}$$

where Q denotes geometric quantities, and we define u as

$$u = \alpha t - \exp(2\phi) r . \tag{2.23}$$

More explicitly, Eq. (2.22) is rewritten as

$$Q(t,r) = \left(1 - \frac{\Delta r}{r}\right) Q(t - \Delta t, r - \Delta r) , \tag{2.24}$$

where Δt is a time step in the simulation, and $\Delta r = \alpha \exp(-2\phi)\Delta t$. In practice, $Q(t-\Delta t, r-\Delta r)$ is obtained by the interpolation from the nearby mesh points. We note that this condition can be interpreted not only as the outgoing boundary condition for the wave, but also as the boundary condition for $1/r$ potential. This is because in the case of $Q(t-\Delta t, r) = Q(t,r) = \text{const}$, Eq. (2.22) becomes $Q(r)r = \text{const}$.

In numerical code, we use the second order finite difference for $\partial/\partial x^i$ such as

$$\frac{\partial}{\partial x} \to \frac{1}{x_{i+1}-x_{i-1}}\left(\frac{Q_{i+1}-Q_i}{x_{i+1}-x_i}(x_i-x_{i-1}) + \frac{Q_i-Q_{i-1}}{x_i-x_{i-1}}(x_{i+1}-x_i)\right),$$
$$\frac{\partial^2}{\partial x^2} \to \frac{2}{x_{i+1}-x_{i-1}}\left(\frac{Q_{i+1}-Q_i}{x_{i+1}-x_i} - \frac{Q_i-Q_{i-1}}{x_i-x_{i-1}}\right). \tag{2.25}$$

The grid points are determined by the rule as

$$\begin{aligned} x_i &= x_{i-1} + w(x_{i-1}-x_{i-2}) , \\ y_j &= y_{j-1} + w(y_{j-1}-y_{j-2}) , \\ z_k &= z_{k-1} + w(z_{k-1}-z_{k-2}) , \end{aligned} \tag{2.26}$$

where w is a constant with $w \geq 1$. The grid covers $-x_{\max} \leq x \leq x_{\max}$, $-y_{\max} \leq y \leq y_{\max}$, and $0 \leq z \leq z_{\max}$. We fix $x_{\max}$, $y_{\max}$, and $z_{\max}$ as $4 \sim 6r_0$, where r_0 is a width of the wave packets (see Sec. III). As for the grid numbers, we take $(N_x, N_y, N_z) = (59, 59, 30)$ mesh points typically. In this case, we use a YHP 715-50 work station. We also perform simulations on the FACOM VP-2600 (in data processing center of Kyoto University) taking (121, 121, 61) mesh points in order to see the dependence on the grid number and resolution, but the results do not change so much. In the typical case, the memory required is about 35 Mbytes and the computational time on a YHP 715-50 work station is about 10 h for 2000 time steps.

For the numerical time evolution, we put $\tilde{\gamma}_{ij}$, F_i, ϕ, and α on t, $t+\Delta t$, $t+2\Delta t$, ... and put $\hat{A}_{ij}$ and K on $t+0.5\Delta t$, $t+1.5\Delta t$, ... For the case of the low amplitude wave, the nonlinear terms in the evolution equations are negligible, so that the numerical method of the time evolution becomes essentially equivalent to a leapfrog method [13]. For the case of the high amplitude wave, the method does not become leapfrog because the nonlinear source terms in the evolution equation are not negligible. Thus, in this case, we adopt a smaller time step than that for the linear wave case for improvement of the numerical accuracy.

III. INITIAL CONDITION FOR GRAVITATIONAL WAVES

In this section, we describe the initial condition for pure gravitational waves. To give the initial condition, we must solve the constraint equations, Eqs. (2.3) and (2.4). Using the conformal factor $\psi = \exp(\phi)$, Eq. (2.3) is written as

$$\tilde{\Delta}\psi = \tfrac{1}{8}[\tilde{R}\psi - (\tilde{A}_{ij}\tilde{A}^{ij} - \tfrac{2}{3}K^2)\psi^5] , \tag{3.1}$$

where $\tilde{\Delta} = \tilde{D}_k\tilde{D}^k$ is the Laplacian with respect to $\tilde{\gamma}_{ij}$ and $\tilde{R} = \tilde{R}_k{}^k$. Using $\tilde{D}_i$ instead of D_i, Eq. (2.4) is also rewritten as

$$\tilde{D}_i\hat{A}^i{}_j - \tfrac{2}{3}\psi^6\tilde{D}_jK = 0 , \tag{3.2}$$

where $\hat{A}^i{}_j \equiv \psi^6\tilde{A}^i{}_j$. Note that indices of $\hat{A}^i{}_j$ are raised and lowered by $\tilde{\gamma}^{ij}$ and $\tilde{\gamma}_{ij}$, respectively.

One of the simplest choices to set the initial condition for vacuum Einstein equation is to consider a conformally flat, $\tilde{\gamma}_{ij} = \eta_{ij}$, and $K = 0$ initial condition. In this case, we only need to consider the initial form of the trace-free extrinsic curvature (i.e., $\hat{A}_{ij}$) and the conformal factor. Nakamura and co-workers derived such initial conditions as well as the general solution of the linearized vacuum Einstein equation [12] to compare the numerical solution with the analytical one. (Hereafter we call the solution of this type the TT wave.) The solutions of the linearized TT wave for $\hat{A}_{ij}$ are composed of two independent modes, even and odd parity modes. In this paper, however, we consider only the even parity mode of the TT waves, which is written as

$$\hat{A}_{ij} = \sum_{lm}\begin{pmatrix} a_{lm}Y_{lm} & b_{lm}Y_{lm,\theta} & b_{lm}Y_{lm,\varphi} \\ * & g_{lm}Y_{lm} + f_{lm}W_{lm} & f_{lm}X_{lm} \\ * & * & (g_{lm}Y_{lm} - f_{lm}W_{lm})\sin^2\theta \end{pmatrix} , \tag{3.3}$$

where an asterisk denotes the relations of symmetry. a_{lm}, b_{lm}, g_{lm}, and f_{lm} are functions of r and t which is described as

$$\begin{aligned} a_{lm} &= r^{l-2}\left(\frac{1}{r}\frac{\partial}{\partial r}\right)^l \frac{P_{lm}(t-r)+Q_{lm}(t+r)}{r}, \quad g_{lm} = -\frac{r^2}{2}a_{lm} , \\ b_{lm} &= \frac{1}{l(l+1)r}\frac{\partial}{\partial r}(r^3a_{lm}), \quad f_{lm} = \frac{1}{(l-2)(l+1)}\left[g_{lm} + \frac{\partial}{\partial r}\left(\frac{r}{l(l+1)}\frac{\partial}{\partial r}(r^3a_{lm})\right)\right] , \end{aligned} \tag{3.4}$$

where P and Q are arbitrary functions. Y_{lm} is the spherical harmonic function, and X_{lm} and W_{lm} are given as

$$X_{lm} = 2\frac{\partial}{\partial\varphi}\left(\frac{\partial}{\partial\theta} - \cot\theta\right)Y_{lm}, \quad W_{lm} = \left(\frac{\partial^2}{\partial\theta^2} - \cot\theta\frac{\partial}{\partial\theta} - \frac{1}{\sin^2\theta}\frac{\partial^2}{\partial\varphi^2}\right)Y_{lm} . \tag{3.5}$$

We use $\hat{A}_{ij}$ at $t = 0$ as the initial condition.

In this paper, we only consider the quadrupole mode ($l = |m| = 2$) for initial conditions. Even in this case, various choices for P_{22}, P_{2-2} and Q_{22}, Q_{2-2} are possible. As one choice, we select

$$P_{22} = P_{2-2} = \frac{C}{4}\sqrt{\frac{32\pi}{15}}\frac{\partial}{\partial t}\exp\left(-\frac{(r-t)^2}{2r_0^2}\right) , \quad Q_{22} = Q_{2-2} = -\frac{C}{4}\sqrt{\frac{32\pi}{15}}\frac{\partial}{\partial t}\exp\left(-\frac{(r+t)^2}{2r_0^2}\right) , \tag{3.6}$$

where C and r_0 denote an arbitrary amplitude of the TT wave and a width of the wave packet. For simplicity, hereafter, we set $r_0 = 1$, i.e., we fix the unit of the length scale to the width of the wave packet. In this case, components of $\hat{A}_{ij}$ at $t = 0$ are written as

$$\begin{aligned}
\hat{A}_{xx} &= C_{12}\exp(-r^2/2)[12 - 8y^2 - 16z^2 + 2z^4 + z^2(x^2 + 3y^2) + y^4 - x^2y^2] , \\
\hat{A}_{yy} &= C_{12}\exp(-r^2/2)[-12 + 8x^2 + 16z^2 - 2z^4 - z^2(3x^2 + y^2) - x^4 + x^2y^2] , \\
\hat{A}_{zz} &= C_{12}\exp(-r^2/2)(x^2 - y^2)(-8 + 2z^2 + x^2 + y^2) , \\
\hat{A}_{xy} &= C_{12}\exp(-r^2/2)xy(x^2 - y^2) , \\
\hat{A}_{xz} &= C_{12}\exp(-r^2/2)xz(12 - 2r^2 + x^2 - y^2) , \\
\hat{A}_{yz} &= C_{12}\exp(-r^2/2)yz(-12 + 2r^2 + x^2 - y^2) ,
\end{aligned} \tag{3.7}$$

where $C_{12} = C/12$. We also consider another set of P and Q as

$$\begin{aligned}
P_{22} = P_{2-2} &= \frac{C'}{2}\sqrt{\frac{32\pi}{15}}\frac{\partial}{\partial t}\left[\left\{\left(\frac{r-t}{r_0}\right)^2 + 1\right\}\exp\left(-\frac{(r-t)^2}{2r_0^2}\right)\right] , \\
Q_{22} = Q_{2-2} &= -\frac{C'}{2}\sqrt{\frac{32\pi}{15}}\frac{\partial}{\partial t}\left[\left\{\left(\frac{r+t}{r_0}\right)^2 + 1\right\}\exp\left(-\frac{(r+t)^2}{2r_0^2}\right)\right] ,
\end{aligned} \tag{3.8}$$

where C' and r_0 also denote an amplitude and a width of the wave packet. We also set $r_0 = 1$. Then, components of $\hat{A}_{ij}$ at $t = 0$ are written as

$$\begin{aligned}
\hat{A}_{xx} &= C'_{12}\exp(-r^2/2)\{-60 + 124z^2 + 12x^2 + 68y^2 - 4z^2 - 17y^4 + x^2y^2 \\
&\quad + z^2(5x^2 - 21y^2) - 30r^2z^2 + 2r^4z^2 - r^2(x^2 - y^2)(y^2 + z^2)\} , \\
\hat{A}_{yy} &= C'_{12}\exp(-r^2/2)\{60 - 124z^2 - 68x^2 - 12y^2 + 4z^2 + 17x^4 - x^2y^2 \\
&\quad + z^2(21x^2 - 5y^2) + 30r^2z^2 - 2r^4z^2 - r^2(x^2 - y^2)(x^2 + z^2)\} , \\
\hat{A}_{zz} &= C'_{12}\exp(-r^2/2)(x^2 - y^2)(56 - 17r^2 - 9z^2 + r^4 + r^2z^2) , \\
\hat{A}_{xy} &= C'_{12}\exp(-r^2/2)xy(x^2 - y^2)(r^2 - 9) , \\
\hat{A}_{xz} &= C'_{12}\exp(-r^2/2)xz\{-84 + 30r^2 - 2r^4 + (r^2 - 9)(x^2 - y^2)\} , \\
\hat{A}_{yz} &= C'_{12}\exp(-r^2/2)yz\{84 - 30r^2 + 2r^4 + (r^2 - 9)(x^2 - y^2)\} ,
\end{aligned} \tag{3.9}$$

where $C'_{12} = C'/12$. Hereafter we call the former [Eq. (3.7)] and the latter [Eq. (3.9)] initial conditions models (A) and (B), respectively. Since exchange between $x \leftrightarrow y$ corresponds to exchange $C(C') \leftrightarrow -C(C')$, it is sufficient to consider the cases of $C, C' > 0$.

Once $\hat{A}_{ij}$ is obtained, we can solve the Hamiltonian constraint as follows:

$$\Delta_{\rm flat}\psi = -\tfrac{1}{8}\psi^{-7}\hat{A}_{ij}\hat{A}^{ij} , \tag{3.10}$$

where $\Delta_{\rm flat}$ is the Laplacian with respect to η_{ij}. This equation is solved under the boundary condition

$$\psi = 1 + \frac{M}{2r} + O(r^{-3}) , \tag{3.11}$$

where M is the gravitational mass of the system. Numerically, we use the following standard method. (1) We put the trial value of ψ in the right-hand side (RHS) of Eq. (3.10). (2) We solve the Poisson equation for a given source term by the Incomplete Choleskii & Conjugate Gradients (ICCG) method [14]. (3) We put new ψ in the RHS of Eq. (3.10). We continue these procedures until a sufficient convergence is achieved. After ψ is obtained, $\tilde{A}_{ij}$ is given by

$$\tilde{A}_{ij} = \psi^{-6}\hat{A}_{ij} . \tag{3.12}$$

IV. SLICE CONDITIONS

We have tried to calculate the dynamical evolution of the TT wave using several slicing conditions. We summarize their properties in this section.

A. Geodesic slice: $\alpha = 1$

Nakamura and co-workers have already solved the evolution of the low amplitude TT wave up to $t \sim x_{\max}$ successfully using the geodesic slice [12]. However, the geodesic slice has been well known as an inappropriate slicing condition because it does not have the singularity avoidance property for black hole formation problems [15]. We here show that for a long time integration, it is also inappropriate to compute the dynamical evolution of the TT wave even if the amplitude of it is low. Let us explain this using the variable K as an example. In the case of the geodesic slice, $\alpha = 1$, Eq. (2.13) becomes

$$\frac{\partial K}{\partial t} = \tilde{A}_{ij}\tilde{A}^{ij} + \frac{1}{3}K^2 \ . \tag{4.1}$$

For low amplitude waves, $\tilde{A}_{ij}$ is regarded as gravitational waves, so even if they initially exist in the central region, in a little while, they must disperse to infinity. Although $K = 0$ initially (at $t = 0$), K becomes positive for $t > 0$ due to the term $\tilde{A}_{ij}\tilde{A}^{ij} > 0$. After gravitational waves ($\tilde{A}_{ij}$) disperse, K obeys the equation as

$$\frac{\partial K}{\partial t} = \frac{1}{3}K^2 \ . \tag{4.2}$$

The solution of it is immediately obtained as

$$K = \frac{3K_1}{3 - K_1(t - t_1)} \ , \tag{4.3}$$

where K_1 denotes K at $t = t_1 > 0$. From the above argument, K_1 will be positive, so that K will diverge at $t \sim t_1 + 3/K_1$. Clearly, this indicates the appearance of the coordinate singularity. Therefore, we can conclude that the geodesic slice is not appropriate even for the evolution of the low amplitude TT waves[1] [see also Fig. 3(a)].

B. Harmonic slice and similar algebraic slices

Next, we consider the slicing condition such as

$$\alpha = \alpha_0(\mathbf{r}) \exp(n\phi) \ , \tag{4.4}$$

where n is a constant and $\alpha_0(\mathbf{r})$ is an arbitrary function of $\mathbf{r}$ which is set initially. In the case of $n = 6$, the slice becomes the harmonic slice with $\beta^i = 0$ [10]. Substituting Eq. (4.4) into Eq. (2.12), we obtain

$$\frac{\partial}{\partial t}\alpha^{-1} = \frac{n}{6}K \ . \tag{4.5}$$

From Eqs. (2.13) and (4.5), we obtain

$$\frac{\partial^2 \alpha}{\partial t^2} = \left(\frac{\partial \alpha}{\partial t}\right)^2 \alpha^{-1} + \frac{n}{6}\alpha^2 \left[-\alpha \left(\tilde{A}_{ij}\tilde{A}^{ij} + \frac{1}{3}K^2 \right) + D^i D_i \alpha \right] \ . \tag{4.6}$$

Let us consider the case of the linear TT waves, and expand geometric variables as

$$\begin{aligned} \tilde{\gamma}_{ij} &= \eta_{ij} + \epsilon h^{(1)}_{ij} \ , \\ \tilde{A}_{ij} &= \epsilon \tilde{A}^{(1)}_{ij} \ , \\ K &= \epsilon^2 K^{(2)} \ , \\ \alpha &= 1 + \epsilon^2 \alpha^{(2)} \ , \end{aligned} \tag{4.7}$$

where ϵ is a small parameter. Then, for the lowest order in $\epsilon(O(\epsilon^2))$, Eq. (4.6) becomes

$$\frac{\partial^2 \alpha^{(2)}}{\partial t^2} = \frac{n}{6}\left(\Delta_{\rm flat}\alpha^{(2)} - \tilde{A}^{(1)}_{ij}\tilde{A}^{(1)}_{ij} \right) \ . \tag{4.8}$$

For $n < 0$, Eq. (4.8) becomes a 4D elliptic type equation. In this case, we can expect that the system is unstable for numerical time evolution. This is because the local dispersion relations for homogeneous equation of Eq. (4.8) become

$$\omega = \pm i \sqrt{\frac{|n|\mathbf{k}\cdot\mathbf{k}}{6}} \ , \tag{4.9}$$

where the Fourier expansion of $\alpha^{(2)}$ by $\exp(i\omega t - i\mathbf{k}\cdot\mathbf{r})$ is assumed. Since unstable modes [i.e., $\mathrm{Im}(\omega) < 0$] always exist, any slicing conditions with $n < 0$ will not be appropriate to evolve the spacetime numerically. This fact can be also applied to the conformal slice [9]

$$\alpha = \exp\left(-2\bar{\psi} - \frac{2}{3}\bar{\psi}^3 - \frac{2}{5}\bar{\psi}^5 \right) \ , \tag{4.10}$$

where $\bar{\psi} = \exp(\phi) - 1$. In this case, the evolution equation in $O(\epsilon^2)$ is written as

$$\frac{\partial^2 \alpha^{(2)}}{\partial t^2} = -\frac{1}{3}\left(\Delta_{\rm flat}\alpha^{(2)} - \tilde{A}^{(1)}_{ij}\tilde{A}^{(1)}_{ij} \right) \ , \tag{4.11}$$

or

$$\frac{\partial^2 \psi^{(2)}}{\partial t^2} = -\frac{1}{3}\left(\Delta_{\rm flat}\psi^{(2)} + \frac{1}{2}\tilde{A}^{(1)}_{ij}\tilde{A}^{(1)}_{ij} \right) \ . \tag{4.12}$$

Since Eq. (4.12) is the same as Eq. (4.8) with $n = 2$ and the RHS of Eq. (4.12) does not vanish even if we use the Hamiltonian constraint, it is unstable for long time numerical evolutions. Therefore, the conformal slice is not appropriate for the time evolution of the TT wave.

[1] Note that if we choose an appropriate K initially, this coordinate singularity may be escaped.

For $n > 0$, Eq. (4.8) is a hyperbolic equation with the source term, $-\tilde{A}^{(1)}_{ij}\tilde{A}^{(1)}_{ij}$. In particular, in the case of $n = 6$, i.e., for the harmonic slice, it becomes the wave equation of the phase velocity = the light velocity. In contrast to $n < 0$ cases, the slice with $n > 0$ seems to allow the stable long time evolution in numerical simulations adopting Eqs. (2.11)–(2.14) and Eq. (2.20). Indeed, we try to calculate the time evolution of the TT wave for a variety of initial conditions and for various $n(= 2, 6, 12)$, and see the stable time evolution of the TT wave. From the various calculations using different $n(> 0)$, we do not find noticeable differences of results (but, the slice with larger n seems to have a stronger singularity avoidance). Therefore in this paper, we mainly use the harmonic slice as an example.

Even if we fix $n = 6$, another freedom remains; choice of $\alpha_0(\mathbf{r})$. For a low amplitude TT wave, its choice is not important, but in a case of higher amplitude TT waves, in particular, for the cases in which the collapse of the TT wave by its self-gravity leads to the high density peaks in the central region or the collapse of the TT wave results in a black hole formation, its choice seems to be important. In Sec. V, we mention the importance of the choice of $\alpha_0(\mathbf{r})$ in more detail.

C. Maximal slice

The maximal slice, $K = 0$, is well known because of the singularity avoidance property for various problems [15,16,11,17]. In the case of the maximal slice, the equation for α becomes

$$\tilde{\Delta}\alpha + 2\tilde{D}_i\phi\tilde{D}^i\alpha = \alpha \exp(4\phi)\tilde{A}_{ij}\tilde{A}^{ij} \ . \tag{4.13}$$

We solve this equation by the relaxation method as follows. (1) We rewrite the equation as

$$\Delta_{\rm flat}\alpha = -(f^{ij}\alpha_{,i})_{,j} - 2\tilde{\gamma}^{ij}\phi_{,i}\alpha_{,j} + \alpha \exp(4\phi)\tilde{A}_{ij}\tilde{A}^{ij} \ . \tag{4.14}$$

(2) We first substitute the trial value of α in the RHS of Eq. (4.13), and by ICCG method we solve the Poisson equation with the boundary condition as

$$\alpha = 1 - \frac{M_a}{r} + O(r^{-3}) \ , \tag{4.15}$$

where

$$M_a = M_a(t) = \lim_{r\to\infty} \frac{1}{4\pi} \oint \nabla_i \alpha \, dS^i \ . \tag{4.16}$$

(3) We continue the above procedure until α converges.

We try to test the convergence for several numerical simulations of the evolution of the TT wave. For the low amplitude TT wave, the convergence of the relaxation is fast. (Note, however, that even in this case, the computational time is about ten times as long as that by means of the harmonic slice for our typical simulations on a work station.) For the higher amplitude TT wave, the convergence of the relaxation becomes slow. This seems due to the first and second terms in the RHS of Eq. (4.14). To overcome this, we need to find a more suitable method to solve Eq. (4.13). For these reasons, in the following calculations, we mainly consider the harmonic slice.

V. NUMERICAL RESULTS

A. Method for analysis

To see some density of gravitational waves, we make use of the curvature invariant as

$$I = 8E_{ij}E^{ij} + 4P_{ijk}P^{ijk} \ , \tag{5.1}$$

where

$$E_{ij} = R_{ij} + KK_{ij} - K_{ik}K^k{}_j \ ,$$
$$P_{ijk} = D_jK_{ik} - D_iK_{jk} \ . \tag{5.2}$$

I is the so-called Bel-Robinson energy density. Since I is a gauge-invariant quantity as well as positive definite, it will be able to extract a physical energy density of gravitational waves.

To see the wave form of gravitational waves, we use the gauge-invariant wave extraction technique, which has recently developed by NCSA group [11]. Following their method, we assume that the numerically calculated spacetime metric near the outer boundary can be split as[2]

$$g_{\mu\nu} = \eta_{\mu\nu} + \xi_{\mu\nu} \ , \tag{5.3}$$

where $\xi_{\mu\nu} = \sum_{lm} \xi^{lm}_{\mu\nu}$ and

$$\xi^{lm}_{\mu\nu} = \begin{pmatrix} H_{0lm}Y_{lm} & H_{1lm}Y_{lm} & h_{0lm}Y_{lm,\theta} & h_{0lm}Y_{lm,\varphi} \\ * & H_{2lm}Y_{lm} & h_{1lm}Y_{lm,\theta} & h_{1lm}Y_{lm,\varphi} \\ * & * & r^2(K_{lm}Y_{lm} + G_{lm}W_{lm}) & r^2G_{lm}X_{lm} \\ * & * & * & r^2\sin^2\theta(K_{lm}Y_{lm} - G_{lm}W_{lm}) \end{pmatrix} \ , \tag{5.4}$$

[2]In the original method of NCSA group, they choose the background metric as the Schwarzschild metric because they consider the spacetime in which a black hole exists in the central region. In this paper, we choose the background metric as the flat one because we apply this method only to the spacetime without black hole.

and H_{0lm}, H_{1lm}, H_{2lm}, h_{0lm}, h_{1lm}, K_{lm}, and G_{lm} are functions of r and t. These variables are calculated from the numerical data of metric tensor as

$$
\begin{aligned}
H_{0lm} &= \int d\Omega\, Y^*_{lm}\alpha^2 \ , \\
H_{2lm} &= \int d\Omega\, Y^*_{lm}\exp(4\phi)\tilde{\gamma}_{rr} \ , \\
h_{1lm} &= \frac{1}{l(l+1)}\int d\Omega\, \exp(4\phi)\left(Y^*_{lm,\theta}\tilde{\gamma}_{r\theta} + \frac{Y^*_{lm,\varphi}}{\sin^2\theta}\tilde{\gamma}_{r\varphi}\right) \ , \\
G_{lm} &= \frac{1}{2(l-1)l(l+1)(l+2)}\int d\Omega\, \exp(4\phi) r^{-2}\left(W^*_{lm}\tilde{\gamma}_{-} + 2X^*_{lm}\frac{\tilde{\gamma}_{\theta\varphi}}{\sin^2\theta}\right) \ , \\
K_{lm} &= \frac{1}{2}\int d\Omega\, Y^*_{lm}\exp(4\phi)\tilde{\gamma}_{+} r^{-2} \ ,
\end{aligned}
\tag{5.5}
$$

where $d\Omega = \sin\theta\, d\theta\, d\varphi$, Y^*_{lm} denotes the complex conjugate of Y_{lm}, and

$$
\tilde{\gamma}_{\pm} = \tilde{\gamma}_{\theta\theta} \pm \frac{\tilde{\gamma}_{\varphi\varphi}}{\sin^2\theta} \ . \tag{5.6}
$$

Note that $H_{1lm} = h_{0lm} = 0$ in the present gauge condition. In practice, $\tilde{\gamma}_{rr}, \tilde{\gamma}_{r\theta}, \ldots$ are transformed from $\tilde{\gamma}_{xx}, \tilde{\gamma}_{xy}, \ldots$.

Using these variables, the gauge-invariant quantity for gravitational waves can be written as

$$
\begin{aligned}
R_{lm}(t,r) = &\sqrt{\frac{2}{(l-1)l(l+1)(l+2)}} \\
&\times(4k_{2lm} + l(l+1)k_{1lm}) \ ,
\end{aligned}
\tag{5.7}
$$

where

$$
\begin{aligned}
k_{1lm} &= K_{lm} + l(l+1)G_{lm} + 2r\frac{\partial G_{lm}}{\partial r} - 2\frac{h_{1lm}}{r} \ , \\
k_{2lm} &= \frac{H_{2lm}}{2} - \frac{1}{2}\frac{\partial}{\partial r}(r\{K_{lm} + l(l+1)G_{lm}\}) \ .
\end{aligned}
\tag{5.8}
$$

We note that $R_{lm}(t,r)$ obeys the flat-space wave equation as

$$
\left(\frac{\partial^2}{\partial t^2} - \frac{1}{r^2}\frac{\partial}{\partial r}r^2\frac{\partial}{\partial r} + \frac{l(l+1)}{r^2}\right)R_{lm}(t,r) = 0 \ . \tag{5.9}
$$

B. Results

We consider the various initial conditions with $0.01 \le C \le 7$ for model (A) and $0.01 \le C' \le 1$ for model (B). In Fig. 1, the relations between the gravitational mass, M, and $C(C')$ are shown for models (A) and (B). In the case of model (A), the relation $M = M_0C^2$ holds for $C \lesssim 0.3$, where M_0 is a constant $\simeq 0.145$. For $C \sim 2$, the mass is about 50% smaller than the extrapolated value $4M_0$, so that we can expect that for $C \gtrsim 2$, the nonlinearity of the TT wave plays an important role in the dynamical evolution. In the case of model (B), the relation $M = M'_0C'^2$ also holds for $C' \lesssim 0.1$, and $M'_0 \simeq 2.6$. In this model, the ratio of the mass to the extrapolated mass formula becomes less than 50% for $C' \gtrsim 0.5$.

In Fig. 2, we show the time evolution of $h_{yy} = \tilde{\gamma}_{yy} - 1$ and $h_{zz} = \tilde{\gamma}_{zz} - 1$ for $C = 0.01$ of model (A) at a coordinate point, (4.2, 0, 0). This calculation is performed using the harmonic slice with $\alpha_0(\mathbf{r}) = 1$. In order to see the numerical accuracy, we show both numerical and analytical results in the figures. The solid and dotted lines denote the numerical and the analytical results, respectively. Here, the analytical result corresponds to a solution of the linearized Einstein equation. We can see that both results agree well. We also find that after wave disperses, h_{ij} remains zero except for the small numerical errors for a long time. Thus we can conclude that the harmonic slice works well for a long time integration of the low amplitude TT wave. Next, in Figs. 3(a) and 3(b), we also show h_{yy} and h_{zz} for $C = 0.01$ of model (A) at (4.2, 0, 0), but by means of the geodesic slice and the maximal slice. For the case of the geodesic slice, h_{ij} gradually deviates from zero after the wave disperses, and the deviation becomes larger and larger. This bad behavior seems to come from the property of the geodesic

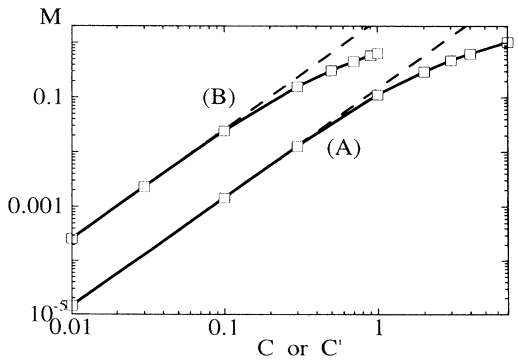

FIG. 1. The relation between the amplitude of the TT wave (C) and the gravitational mass (M) at $t = 0$ for models (A) and (B). The solid and dashed lines denote the gravitational mass and $M = M_0C^2$, respectively. The open squares are the data points by numerical calculations.

slice explained in Sec. IV A, and this clearly shows that the geodesic slice is not appropriate to simulate even the low amplitude TT wave for a long time. On the other hand, the maximal slice works well for this problem.

In Figs. 4(a)–4(d), we show the time evolution of the Bel-Robinson energy density (I) for $C = 0.1$, 2, 4, and 7 of model (A). We also show I for $C' = 0.3$, 0.5, and 1 of model (B) in Figs. 4(e)–4(g) to see whether the difference of the initial condition affects the time evolution of I. The figures denote the density contours of I in the equatorial plane. First, we pay attention to model (A). For $C = 0.1$, we see that the wave only disperses to infinity. In this case, the nonlinearity of the TT wave is not important, so that we may regard the time evolution of I for $C = 0.1$ as a typical behavior of I for the low amplitude TT wave. For $C = 2$, the behavior of I is different from that for the low amplitude TT wave due to the nonlinearity. At early times in the evolution, the wave packet collapses by its self-gravity and high density peaks appear near the origin. Then it disperses to infinity like in the case of $C = 0.1$. For $C = 4$, concentration

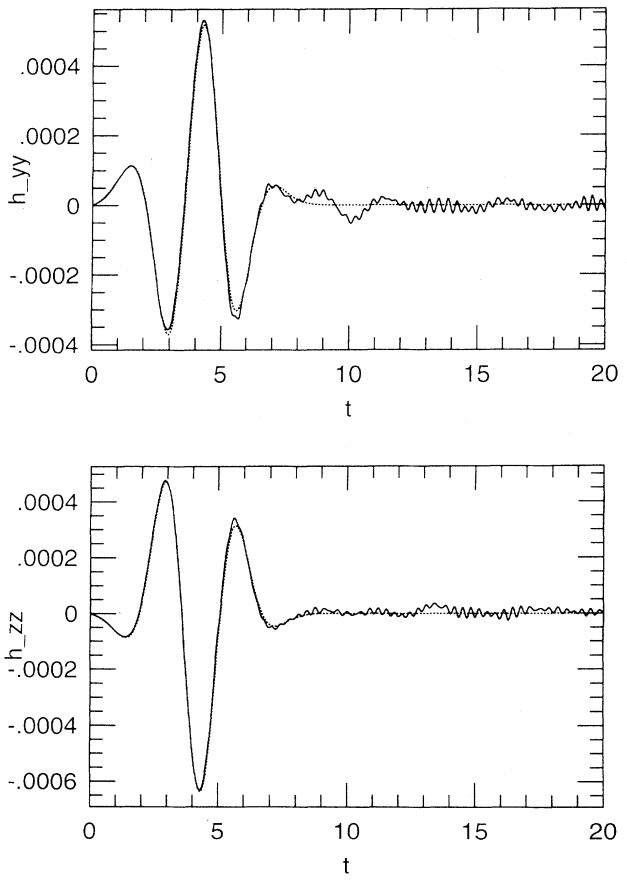

FIG. 2. The time evolution of h_{yy} and h_{zz} for $C = 0.01$ of model (A) at $(x_{\max}, 0, 0)$. In this calculation, we use the harmonic slice with $\alpha_0(\mathbf{r}) = 1$. Solid and dotted lines show the numerical and analytical results, respectively. Here, the analytical results correspond to the solution of the linearized Einstein equation.

of the wave is more remarkable. After the wave packet collapses to the central region, it does not disperse soon, but oscillates around the origin for a few times. In this case, the amplitude of the oscillation is also very high, but the wave disperses after the oscillation. Finally we show I for $C = 7$. In this case, the initial behavior is essentially the same as for $C = 4$. But after the wave packet collapses to the central region, the behavior is different; without oscillations, the wave merely collapses and the amplitude becomes higher and higher. Although we do not try to find the apparent horizon or event horizon in the present simulations, we may expect that a black hole will be formed in the central region like in the case of axisymmetric calculations [17].

Next, we see I for $C' = 0.3$, 0.5, and 1 of model (B) in Figs. 4(e)–4(g). We soon find that features of the time evolution of I for each model is very similar to that for $C = 2$, 4, and 7 of model (A): In the case of $C' = 0.3$, the wave packet first collapses to the central region by its self-gravity and then disperses to infinity. In the case of $C' = 0.5$, after the wave packet collapses to the central region, high amplitude oscillations of the wave continue for a few times, and finally the wave disperses to infinity. In the case of $C' = 1$, once the wave packet collapses, it continues to collapse without oscillating so much. The difference between models (A) and (B) is the steepness of the initial configuration of I in the central region: The initial configuration of I for model (B) are steeper than that for model (A) in the central region even if the gravitational masses of the system are the same. This difference seems to affect the threshold value of $M/r_0 \equiv \sigma_{\rm crit}$, beyond which the wave packet must collapse. In the case of model (A), $\sigma_{\rm crit} \sim 0.5$ for $C \sim 7$, but in the case of model (B), it is slightly different from that for model (A) and becomes about 0.3 for $C' \sim 1$. However, the difference we find is only this point. Initial configurations of the TT wave do not seem to change its final fate extremely.

We note that the above calculations are performed using the harmonic slice with $\alpha_0(\mathbf{r}) = 1$ for $C = 0.1$ of model (A), but for $C = 2$, 4, 7 of model (A) and $C' = 0.3$, 0.5, 1 of model (B), we determine $\alpha_0(\mathbf{r})$ from the relation

$$\frac{\partial K}{\partial t} = 0 \,. \tag{5.10}$$

Thus the initial slice agrees with that determined by the maximal slice condition. Note that for $C = 0.1$ and 2 of model (A) and for $C' = 0.3$ of model (B), i.e., for cases that the amplitude of the TT wave is not so high, we also perform the calculations by using various $\alpha_0(\mathbf{r})$, and obtain essentially the same results. We also try many choices of $\alpha_0(\mathbf{r})$ for $C \gtrsim 4$ of model (A) and for $C' \gtrsim 0.5$ of model (B), but the choice satisfying Eq. (5.10) seems the best of all in the case of high amplitude TT waves. If we use the slicing condition that $\alpha_0(\mathbf{r})$ does not satisfy Eq. (5.10) as an initial condition for the harmonic slice, we obtain the results in which values of geometric variables around the origin become very large and computation breaks down although a true singularity does not appear. This behavior seems due to the appearance of the coordinate singularity. Hence, that does not show a

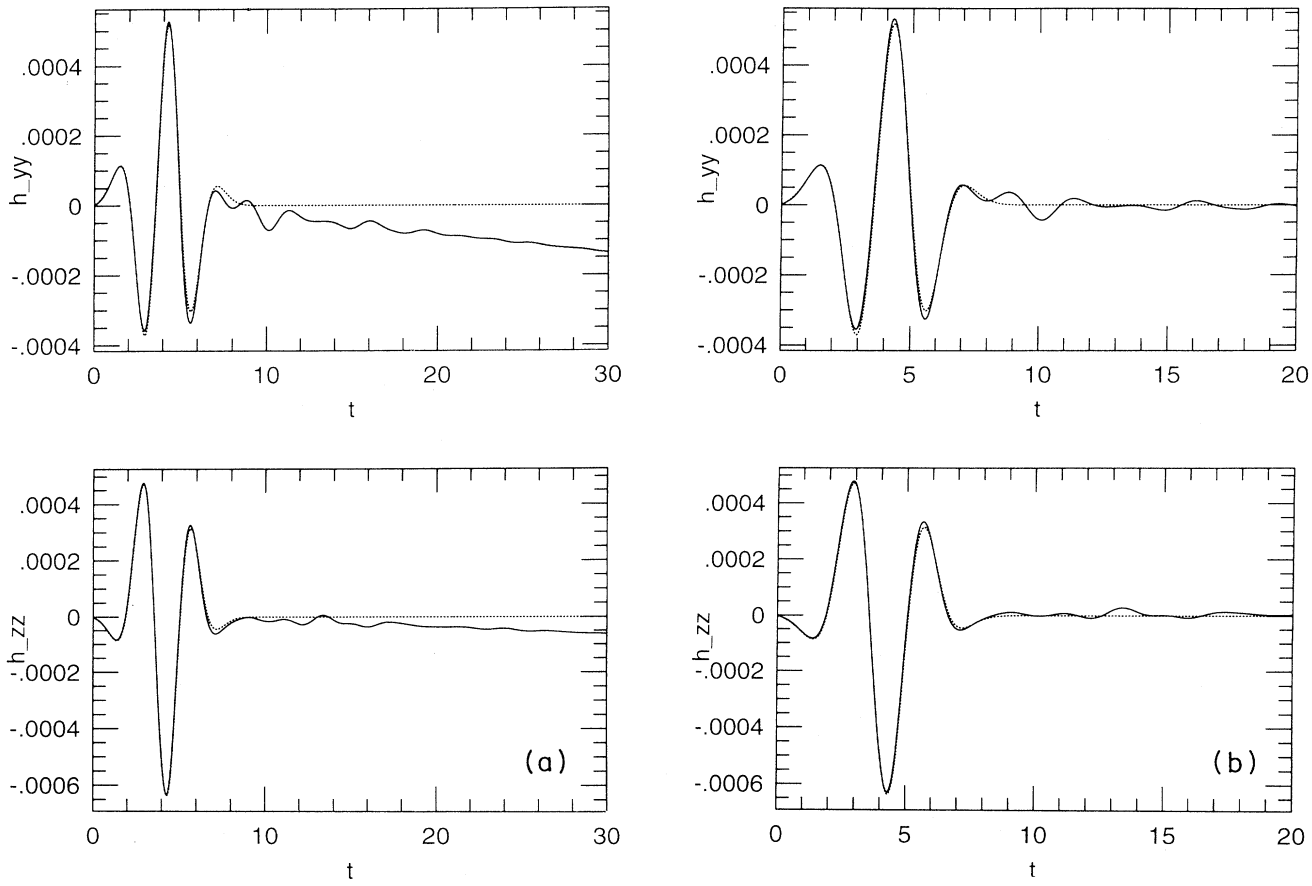

FIG. 3. The same as in Fig. 2 except for the slicing condition; (a) for the geodesic slice and (b) for the maximal slice.

drawback of the harmonic slice because it can be escaped easily by choosing an appropriate initial $\alpha_0(\mathbf{r})$. However, it also shows that we should carefully choose $\alpha_0(\mathbf{r})$ for the highly distorted spacetime such as the high amplitude TT wave.

We should also notice that for $C = 7$ of model (A) and for $C' = 1$ of model (B), i.e., in the case that the TT wave collapses by its self-gravity, the harmonic slice even with Eq. (5.10) does not have the singularity avoidance property: The 3D hypersurface seems to hit the singularity (or approach very near it) soon after the collapse of the TT wave. As we mentioned above, we also perform simulations with other $\alpha_0(\mathbf{r})$, but the results are essentially the same. Bona and Masso [10] proved that the harmonic slice avoids the singularity. In their proof, they assumed that the behavior of α near the singularity is $\alpha(\tau) \sim (\tau_s - \tau)^p$, where τ and τ_s, respectively, denote the proper time of an observer on the normal line and that when the spacetime hits the singularity. From the physical reason, they assumed $p \geq 1$, and in this case, the harmonic slice has the singularity avoidance property because the singularities cannot be reached in a finite coordinate time. However, in this case, we find from Eq. (4.5) $K \to (\tau_s - \tau)^{-1}$. Then, we can easily expect that the other quantities such as $\tilde{A}_{ij}$ also diverge because in the evolution equation of them, K is included [see Eq. (2.11)]. In the numerically generated spacetime, we cannot treat the large value accurately because of a restricted precision of the computer, so that the harmonic slice will not be available near the singularity in a practical simulation.

Furthermore, the harmonic slice seems to have another drawback. In Figs. 5(a) and 5(b), we show the time evolution of α and K near the singularity for $C' = 1$ of model (B) as an example. In the figure, we see that at early time, α does not become small quickly and it becomes small only just before the time slice approaches the singularity. We suspect that the reason for this behavior is due to the structure of the equation for α [see Eq. (4.5)]; if $K > 0$, α becomes small, but if $K < 0$, α becomes large. Since K can become both positive and negative even in the case that the amplitude of the TT wave is high [see Fig. 5(b)], α is not guaranteed to approach zero quickly even when the TT wave begins to collapse. One idea to escape this property may be to adopt following improved slicing conditions instead of the harmonic slice:

$$\frac{\partial \alpha}{\partial t} = \alpha^n (e^K - 1) \ , \tag{5.11}$$

or

$$\frac{\partial \alpha}{\partial t} = -\alpha^n K e^K \ , \tag{5.12}$$

where n is an arbitrary factor ~ 1. The reason why this choice is good is that if $K > 0$, α becomes small and even if $K < 0$, α does not become so large, and also in the case that the amplitude of the TT wave is low (i.e., $|K| \ll 1$), the property of these slicing conditions is expected to be essentially the same as that of the harmonic slice. In any case, the singularity avoidance property of the harmonic slice seems to be weak. This point should be clarified by means of several other calculations in future works.

Next, let us investigate the wave form of the TT wave at an outer region. In Figs. 6(a)–6(d), we show $R_{lm}(t,r)$ for $C = 0.1$, 2 of model (A) and for $C' = 0.03$, 0.3 of model (B). We note that the wave extraction performed at $r = 3.9r_0$ in Figs. 6(a) and 6(c), and $r = 4.6r_0$ in Figs. 6(b) and 6(d). In these figures, the solid, dotted, dashed, long dashed, and dotted-dashed lines denote $(l,m) = (2,2_+),(2,0),(4,4_+),(4,2_+)$, and (4,0) modes. 2_+ and 4_+ denote the combination of mode like $(Y_{l2} + Y_{l-2})/\sqrt{2}$ and $(Y_{l4} + Y_{l-4})/\sqrt{2}$. Note that in the initial slice, only the $(2,2_+)$ mode exists. For $C = 0.1$ of mode (A) and $C' = 0.03$ of model (B), $(2,2_+)$ mode dominates over the other modes throughout the whole time. This is quite natural because the nature of the TT wave is linear and the nonlinear couplings with the other modes are negligible. To check whether the wave extraction works well or not, in Fig. 7 we also write the gauge-invariant wave form of gravitational waves at $r = 3.9r_0$ by the analytical calculation, which is written as

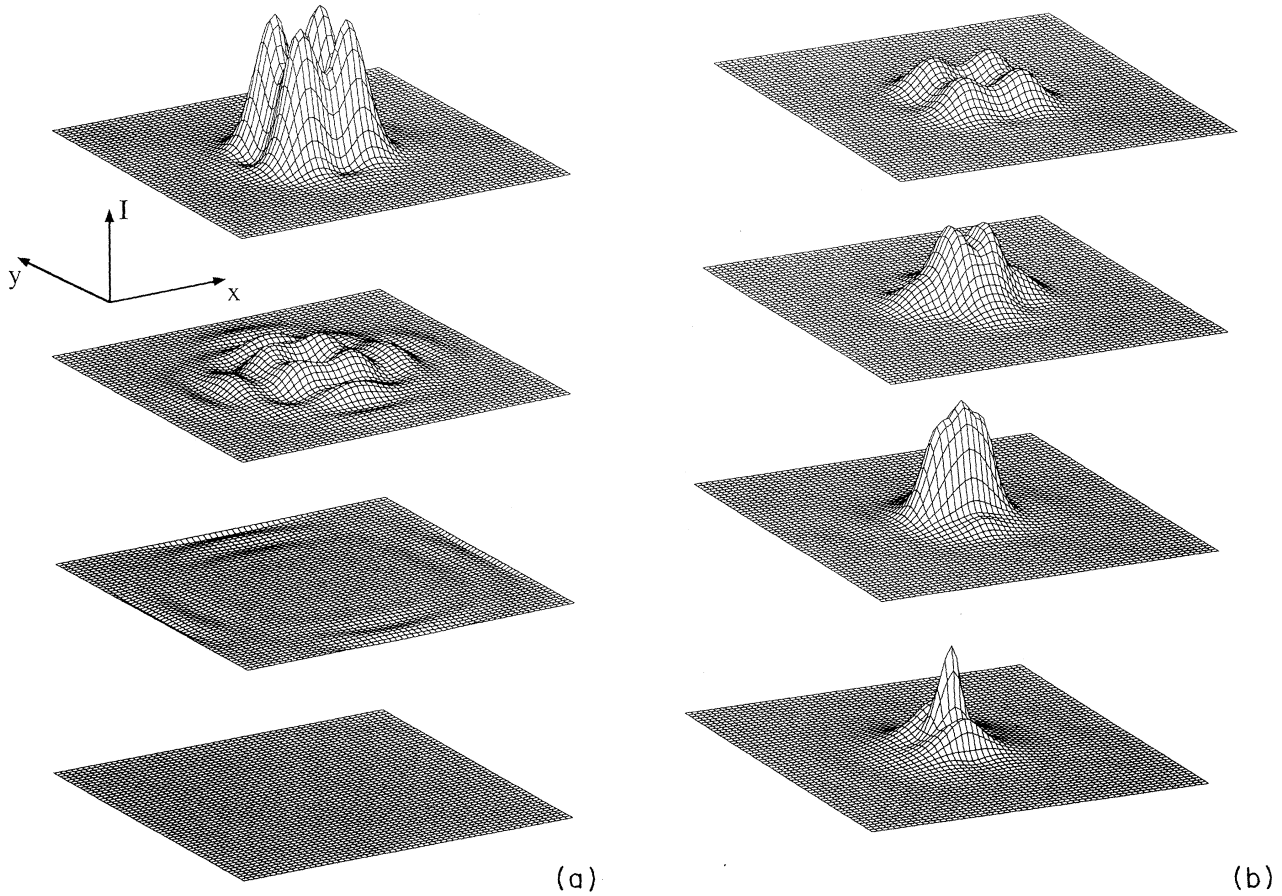

FIG. 4. The contours of the Bel-Robinson's energy density I in the equatorial plane. (a) For $C = 0.1$ of model (A) and for $t = 0$, 2.25, 4.5, 6.75. (b) For $C = 2$ of model (A) and for $t = 0$, 1, 2, 3, 4, 5, 6, 9. (c) For $C = 4$ of model (A) and for $t = 0$, 1, 3, 5, 6, 8, 11, 14. (d) For $C = 7$ of model (A) and for $t = 0$, 4, 6, 7. In this calculation, the 3D hypersurface seems to hit the singularity at $y \sim \pm 1.5$ and $t \gtrsim 7$. (e) For $C' = 0.3$ of model (B) and for $t = 0$, 1, 2, 4, 6. (f) For $C' = 0.5$ of model (B) and for $t = 0$, 1, 2, 3, 4, 5, 6, 8. (g) For $C' = 1$ of model (B) and for $t = 0$, 4, 6, 7, 9. In this calculation, the 3D hypersurface seems to hit the singularity at $x \sim \pm 0.4$ and $t \gtrsim 9$.

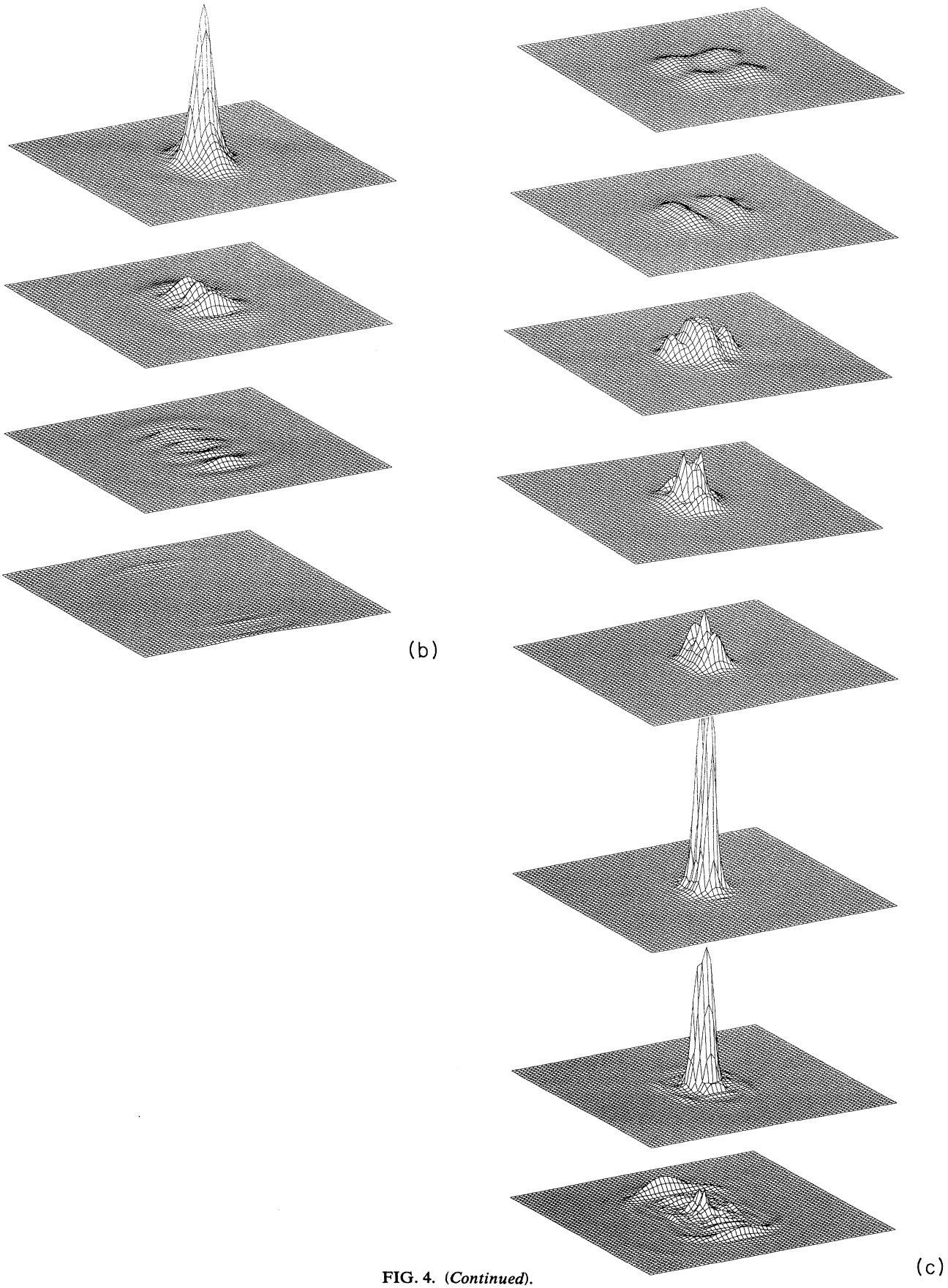

FIG. 4. (*Continued*).

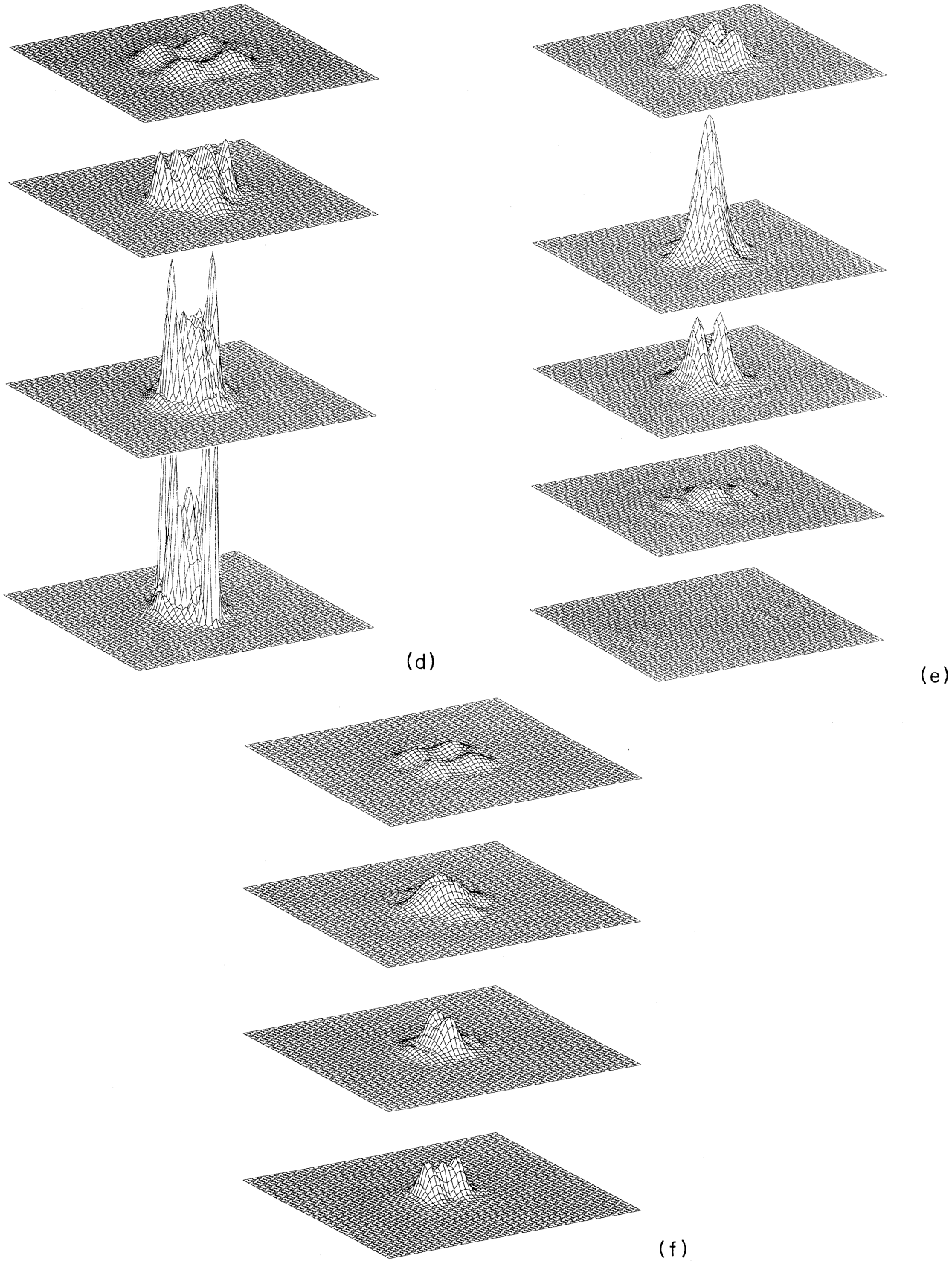

FIG. 4. (*Continued*).

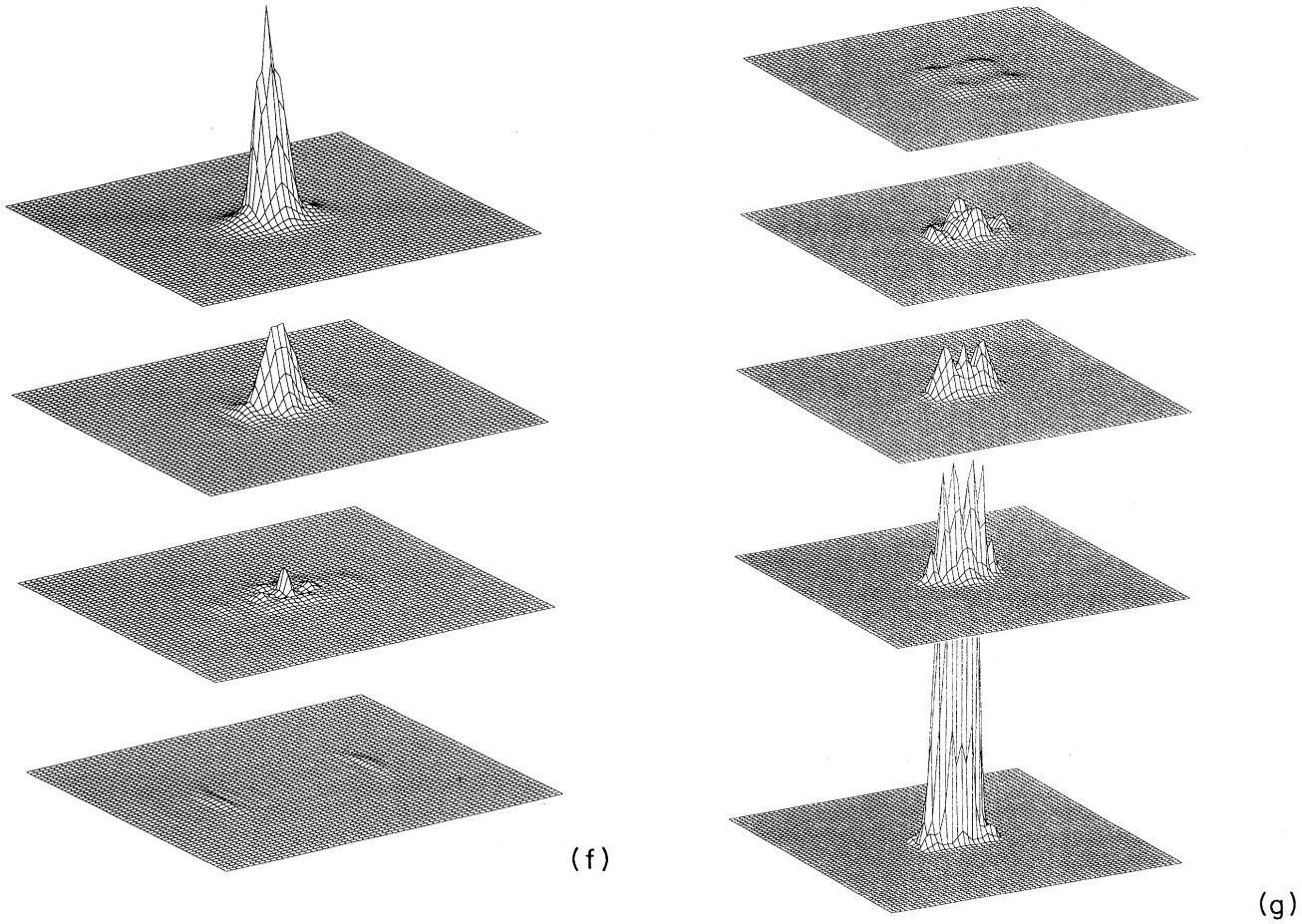

FIG. 4. (*Continued*).

$$R_{22_+} = \sqrt{\frac{16\pi}{15}}\frac{1}{r^3}\left[\exp\left(-\frac{(r+t)^2}{2}\right)(-3-3r^2-3r^4+r^6-3rt-3r^3t+4r^5t\right.$$

$$+3t^2+3r^2t^2+6r^4t^2+3rt^3+4r^3t^3+r^2t^4)+\exp\left(-\frac{(r-t)^2}{2}\right)(3+3r^2+3r^4-r^6-3rt-3r^3t+4r^5t$$

$$\left.-3t^2-3r^2t^2-6r^4t^2+3rt^3+4r^3t^3-r^2t^4)\right]. \tag{5.13}$$

In this figure, the solid and dotted lines denote the numerical and analytical data, respectively, and Fig. 7 shows that they agree well. Therefore, we can consider that the wave extraction technique works well. (We note that the wave form is different from that at infinity. To see that with an accuracy less than $\sim 1\%$, we have to take the grid up to $r \sim$ a few $\times 10 r_0$, but this point is not important in this paper.)

For $C \gtrsim 2$ of model (A) and $C' \gtrsim 0.3$ of model (B), the nonlinearity becomes important; (2, 0) mode has a high amplitude. The ratio of peak amplitudes for (2, 0) mode to $(2, 2_+)$ mode is about several $\times 10\%$ for $C = 2$ of model (A) and $C' = 0.3$ of model (B). Thus the excitation of the higher multipole modes is expected as the amplitude of the TT wave becomes large.

Let us apply the above analysis to the wave form of

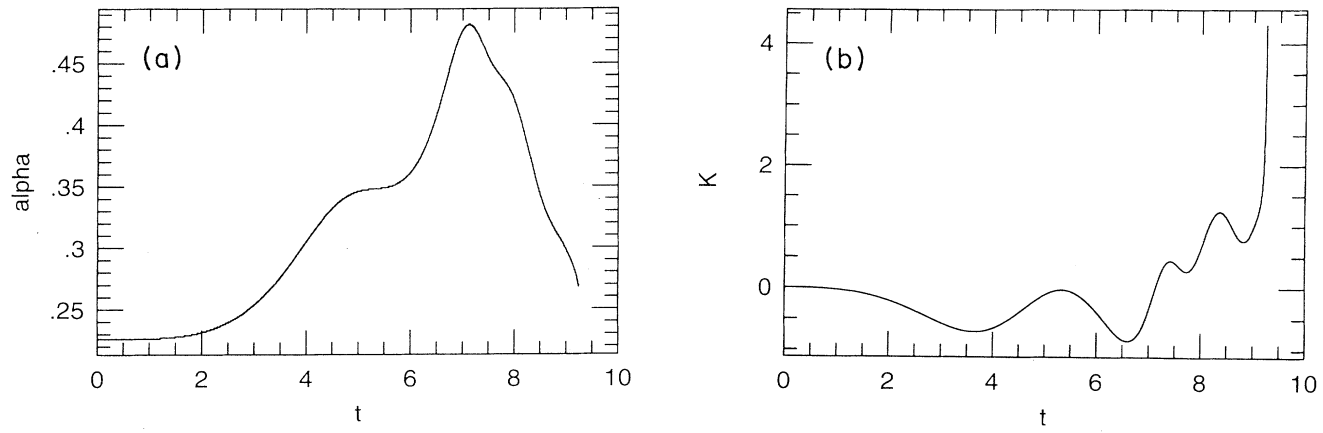

FIG. 5. Time evolution of α (a) and K (b) near the singularity for $C' = 1$ of model (B).

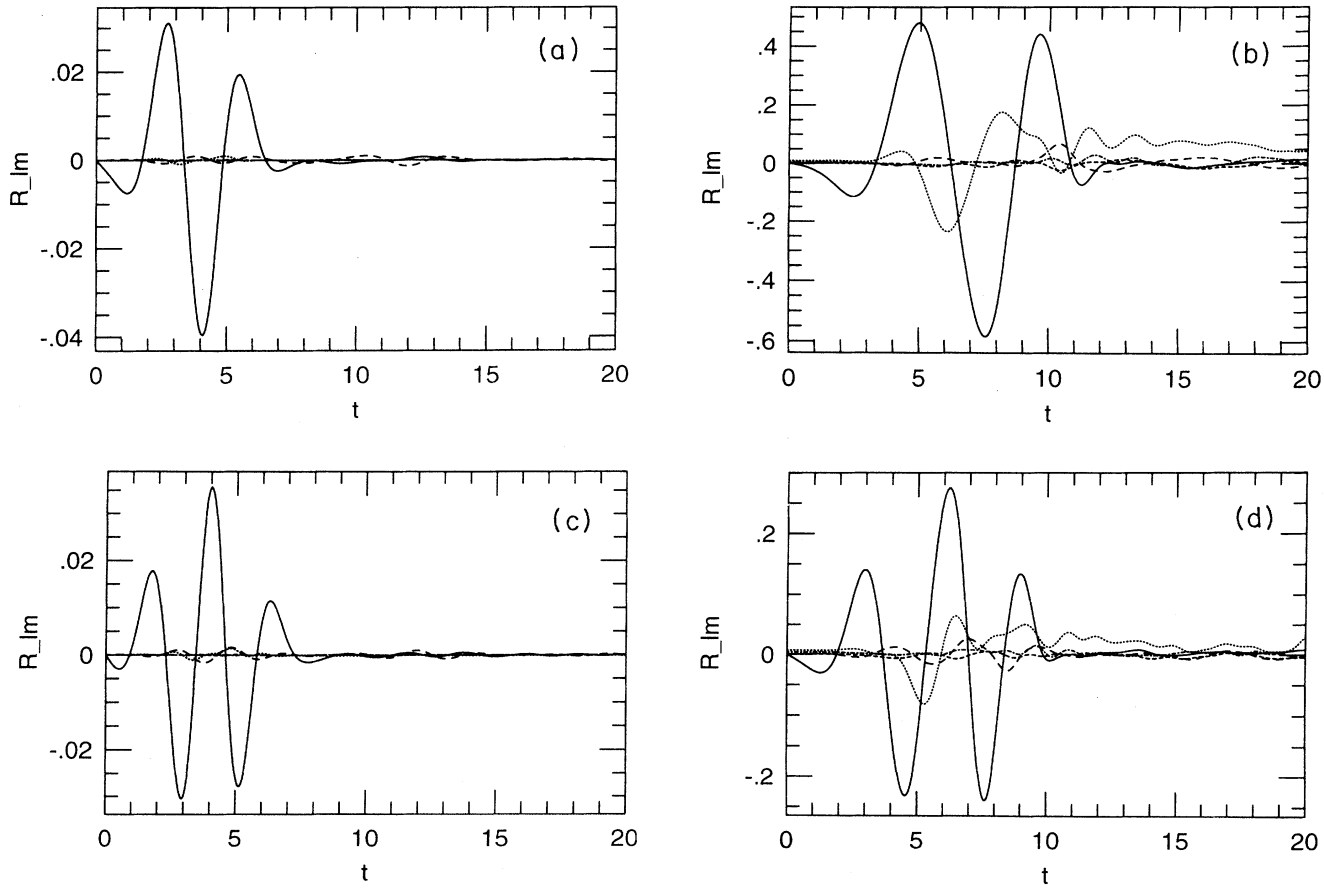

FIG. 6. Several modes of gravitational waves are shown for various initial conditions of models (A) and (B). Gravitational waves are extracted from the gauge-invariant technique. The solid, dotted, dashed, long dashed, and dotted-dashed lines denote $(l, m) = (2, 2_+), (2, 0), (4, 4_+), (4, 2_+)$, and (4,0) modes. 2_+ and 4_+ denote the combination of mode like $(Y_{l2} + Y_{l-2})/\sqrt{2}$ and $(Y_{l4} + Y_{l-4})/\sqrt{2}$. Each figure shows for (a) $C = 0.1$, (b) $C = 2$, and (c) $C' = 0.03$, (d) $C' = 0.3$ of model (B). For (a) and (c), wave extraction is performed at $r = 3.9r_0$ and for (b) and (d), at $r = 4.6r_0$.

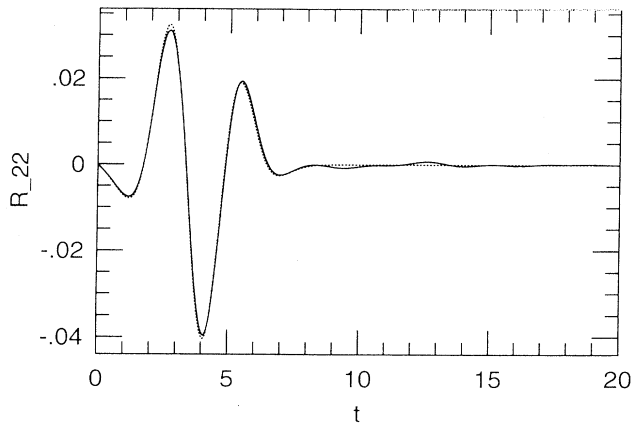

FIG. 7. R_{22_+} at $r = 3.9r_0$ for $C = 0.1$ of model (A) by means of the analytical and numerical calculations. The solid and dotted lines show the numerical and analytical [Eq. (5.13)] results, respectively.

merging compact binaries such as binary neutron stars and binary black holes. At the merging of such binaries, the amplitude of gravitational waves at the Schwarzschild radius of the binaries will be of order unity. In reality, Newtonian 3D numerical simulations [6] showed that its value is about 0.3 for quadrupole gravitational waves. In the present calculation, this value corresponds to that for the cases of $C \sim 1$ or $C' \sim 0.3$, so that a sufficient excitation of the higher multipole modes by the quadrupole mode may occur. This implies that the perturbation analysis [18] may not be appropriate for emission problems of gravitational waves from the merging binary unless the merged object is swallowed inside the event horizon rapidly enough.

VI. SUMMARY

In this paper, we have simulated the dynamical evolution of the vacuum spacetimes of pure gravitational waves. As the initial condition of gravitational waves, we use a conformally flat and $K = 0$ initial condition. (We call this the TT wave in this paper.) We consider both the low and high amplitude TT waves to see the property of several slicing conditions in many types of the spacetime and to show that the gauge-invariant wave extraction technique works well. As for the slicing conditions, we reached the following conclusions.

(1) Geodesic slice: This slice is not appropriate to simulate the evolution of the TT wave for a long time even if its amplitude is low.

(2) Harmonic slice: This slice is appropriate to simulate the evolution of the TT wave for a long time unless the amplitude of the TT wave is too high. However, in the case in which the amplitude of the TT wave is so high that it collapses to a black hole, this slice seems inappropriate: Our simulations indicate the following behaviors. (a) The time slice approaches very near the singularity, so that values of geometric variables become very large (e.g., $K \to \infty$) and numerical calculation cannot follow the subsequent evolution. (b) The lapse function does not become small quickly even when the TT wave begins to collapse. Thus the singularity avoidance property of the harmonic slice seems weak. We must consider a slicing condition in which time slice does not approach the singularity too closely as well as the lapse function approaches zero quickly when the TT wave begins to collapse.

(3) Maximal slice: This slice will have a suitable property to follow the evolution of the TT wave even in the case in which the black hole is formed from the high amplitude TT wave. (This was shown by axisymmetric calculations [17].) However, to use this slice, we must solve a 3D elliptical equation. If we can develop a good method to solve it, this slice will become a useful slicing condition.

We also investigate whether the gauge-invariant wave extraction technique works well or not, and make sure that it is good. By using this technique, we also see the nonlinearity of the Einstein equation: Even if only the quadrupole mode of gravitational waves exists initially, the nonlinearity of the Einstein equation induces the other multipole modes. This means that in the case of the merging of compact binary, nonlinear excitation of the higher multipole modes from the quadrupole mode may be expected. Hence detection of the signal of the last phase of coalescing binary may lead to see the nonlinearity of the Einstein gravity.[3]

In this paper, we have described the numerical results of the dynamical evolution of gravitational waves with even parity and with one wave packet. As a subsequent work, we plan to investigate the dynamical evolution of odd parity gravitational waves or the collision between two wave packets of high amplitude gravitational waves. These subjects can be studied by the present numerical code, so we will be able to report these results in the near future. As in the case of $C = 7$ of model (A) and $C' = 1$ of model (B), high amplitude gravitational waves collapse gravitationally, and probably a black hole is formed. To make sure of it, (1) we must construct the numerical code to find the apparent horizon in general cases [20], and (2) we must find an appropriate slicing condition which has the singularity avoidance property. As for (2), the slicing conditions described by Eqs. (5.11) or (5.12), and the maximal slice may have possibilities. Investigation of these slicing conditions remains as an important future work.

ACKNOWLEDGMENTS

We thank K. Nakao for frequent conversations and useful discussions. This work was in part supported by the Japanese Grant-in-Aid Scientific Research of the Ministry of Education, Science and Culture, Grant Nos. 04234104 and 06740343.

[3]Note that if we can detect the *nonlinear memory* of coalescing binaries, we may also see the nonlinearity of the Einstein gravity [19].

[1] C. Cutler *et al.*, Phys. Rev. Lett. **70**, 2984 (1993).
[2] R. E. Vogt, in *Sixth Marcel Grossmann Meeting on General Relativity*, Proceedings, Kyoto, Japan, 1991, edited by H. Sato and T. Nakamura (World Scientific, Singapore, 1991), p. 244; A. Abramovici *et al.*, Science **256**, 325 (1992); K. S. Thorne, in *Eighth Nishinomiya-Yukawa Memorial Symposium on Relativistic Astrophysics*, Proceedings, edited by M. Sasaki (Universal Academy Press, Tokyo, 1994), p. 67.
[3] C. Bradaschia *et al.*, Nucl. Instrum. Methods Phys. Res. Sect. A **289**, 518 (1990).
[4] C. W. Lincoln and C. M. Will, Phys. Rev. D **42**, 1123 (1990).
[5] D. Lai, F. A. Rasio, and S. L. Shapiro, Astrophys. J. **423**, 344 (1994), and references therein.
[6] For example, M. Shibata, T. Nakamura, and K. Oohara, Prog. Theor. Phys. **88**, 1079 (1992), and references therein.
[7] L. Smarr and J. W. York, Phys. Rev. D **17**, 1945 (1978); **17**, 2529 (1978).
[8] T. Nakamura, in *Eighth Nishinomiya-Yukawa Memorial Symposium on Relativistic Astrophysics*, Proceedings [2], p. 155; in *General Relativity*, Proceedings of the Seventh Marcel Grossmann Meeting on General Relativity, Stanford, California, 1994, edited by R. Ruffini and M. Keiser (World Scientific, Singapore, 1995).
[9] M. Shibata and T. Nakamura, Prog. Theor. Phys. **88**, 317 (1992).
[10] C. Bona and J. Masso, Phys. Rev. D **38**, 2419 (1988); Phys. Rev. Lett. **68**, 1097 (1992).
[11] A. Abrahams, D. Bernstein, D. Hobill, E. Seidel, and L. Smarr, Phys. Rev. D **45**, 3544 (1992); P. Anninos *et al.*, *ibid.* **50**, 3801 (1994); D. Berstein *et al.*, *ibid.* **50**, 5000 (1994), and see references therein.
[12] T. Nakamura, K. Oohara, and Y. Kojima, Prog. Theor. Phys. Suppl. **90**, 76 (1987); T. Nakamura and K. Oohara, *Frontiers in Numerical Relativity*, edited by C. R. Evans, L. S. Finn, and D. W. Hobill (Cambridge University Press, Cambridge, England, 1989), p. 254.
[13] W. H. Press *et al.*, *Numerical Recipes* (Cambridge University Press, Cambridge, England, 1989).
[14] K. Oohara and T. Nakamura, Prog. Theor. Phys. **81**, 360 (1989).
[15] D. M. Eardley and L. Smarr, Phys. Rev. D **19**, 2239 (1979).
[16] S. L. Shapiro and S. A. Teukolsky, in *Eighth Nishinomiya-Yukawa Memorial Symposium on Relativistic Astrophysics*, Proceedings [2], p. 141, and as for their works, see references therein.
[17] M. Shibata, K. Nakao, T. Nakamura, and K. Maeda, Phys. Rev. D **50**, 708 (1994).
[18] R. H. Price and J. Pullin, Phys. Rev. Lett. **72**, 3297 (1994).
[19] K. S. Thorne, Phys. Rev. D **45**, 520 (1992); A. G. Wiseman and C. M. Will, *ibid.* **44**, R2945 (1991); D. Kennefick, *ibid.* **50**, 3587 (1994).
[20] T. Nakamura, Y. Kojima, and K. Oohara, Phys. Lett. **106A**, 235 (1984).